Electrically Controllable Composite Right/ Left-Handed Leaky-Wave Antenna Using Liquid Crystals in PCB Technology

Bang-Jun Che, *Student Member, IEEE*, Tao Jin, Daniel Erni, *Member, IEEE*, Fan-Yi Meng, *Senior Member, IEEE*, Yue-Long Lyu, *Student Member, IEEE*, and Qun Wu, *Senior Member, IEEE*

***Abstract*— A design method for electrically controllable composite right/left-handed (CRLH) leaky-wave antennas (LWAs) with large beam-steering range employing liquid crystal (LC) in printed circuit board technology is proposed. It is demonstrated with detailed mathematical derivation that the design principle enables the LC-CRLH-LWA to keep the balanced condition with all bias states applied to the LC, yielding LC-CRLH-LWAs that feature a steady balanced condition and a broadband property. Based on this principle, an LC-CRLH-LWA prototype is designed, simulated, optimized, and experimentally validated. According to the simulation results, the designed LC-CRLH-LWA operates in the band from 11.14 to 12.77 GHz with a frequency-agile radiation direction. By tuning the permittivity of LC, the radiation direction of the designed antenna scans from -21° to $+23^\circ$ at the fixed operating frequency of 12.4 GHz. The experimental results agree well with the simulated data. Furthermore, sidelobe level suppression of the designed antenna is achieved through decreasing the reflection between the unit cells of the antenna.**

***Index Terms*— Composite right/left-handed (CRLH), electrically beam-steering, large beam steering range, leaky-wave antenna (LWA), liquid crystal (LC), steady balanced condition.**

I. Introduction

LEAKY-WAVE antennas (LWAs) based on composite right/left-handed transmission line (CRLH-TL) have become a research hotspot due to their attractive properties such as continuous beam scanning from backward to forward, low profile, high directivity, compact structure, and low cost [1]–[9]. However, the frequency-beam-scanning property of LWAs has limited their applications in modern communication systems, which generally require fixed-frequency operation for effective channelizing. In the past decades, significant efforts have been made toward developing fixed-frequency beam-scanning LWAs [10]–[16]. For instance, LWAs based on ferrite are reported in [11] and [16], whose radiation direction is tuned by the external static magnetic field. Electrically controllable LWAs based on p-i-n diodes or varactor diodes are also proposed [12]–[15], whose beam steering is realized by adjusting the bias voltage applied to the diodes. Compared to the magnetically beam-steering LWAs, the electrically controllable ones rely on a much smaller and simpler control device that is more feasible for integrated systems and mobile devices. However, such LWA beam steering based on diodes is generally limited to low-frequency application under 10 GHz due to the cumulative effect of the diode parasitics at high frequencies [17].

Electrically controllable LWAs based on liquid crystal (LC) were recently proposed for high-frequency applications [18]–[24]. The LC material is a kind of tunable dielectric whose permittivity tensor can be artificially controlled by the static magnetic or electric bias field [25]–[38]. Consequently, the radiation angle of the LC–LWAs is steered with the tunable permittivity encountered by the RF electric field. Nevertheless, the reported LC–LWAs either demand a strong magnetic bias field, whose generation device is bulky and presents high loss [19], or provide only a small beam-steering range [18], [20]–[24], which limits the application of LC–LWAs in modern wireless communication and radar systems. Up to date, no method for achieving the electrically controllable LC–LWA with large beam-steering range is reported. The LC–LWA whose radiation direction scans agilely versus frequency is promised to generate a large electrically beam steering range. However, the frequency-agile radiation direction is generally associated with narrow bandwidth [39]–[41]. For a tunable LWA, its bandwidth is determined by the common bandwidth of the two typical states [10]–[16]. Consequently, the narrow bandwidth for each state will result in a narrow bandwidth of the tunable LWA. Besides, the balanced condition of such CRLH-TLs-based LC–LWAs is inclined to be broken as the permittivity of the LC varies with the bias voltage, which significantly deteriorates the broadside radiation performance and the corresponding return loss [20]–[24].

Manuscript received December 4, 2016; revised February 17, 2017; accepted February 28, 2017. Date of publication March 28, 2017; date of current version August 14, 2017. This work was supported by the National Natural Science Fund of China under Grant 61671180. Recommended for publication by Associate Editor A. Orlandi upon evaluation of reviewers' comments. *(Corresponding author: Fan-Yi Meng.)*

B.-J. Che and Y.-L. Lyu are with the Harbin Institute of Technology, Harbin 150001, China (e-mail: chebangjun1991@163.com; lvyue-longlvyuelong@126.com).

T. Jin is with the Department of Electronic Information Engineering, School of Information and Electrical Engineering, Harbin Institute of Technology, Weihai 264209, China (e-mail: jintao@hit.edu.cn).

D. Erni is with the Faculty of Engineering, Laboratory for General and Theoretical Electrical Engineering and the CENIDE-Center for Nanointegration Duisburg-Essen, University of Duisburg-Essen, 47048 Duisburg, Germany (e-mail: daniel.erni@uni-due.de).

F.-Y. Meng and Q. Wu are with the Department of Microwave Engineering, Harbin Institute of Technology, Harbin 150001, China (e-mail: blade@hit.edu.cn; fymenghit@gmail.com; qwu@hit.edu.cn).

Color versions of one or more of the figures in this paper are available online at http://ieeexplore.ieee.org.

Digital Object Identifier 10.1109/TCPMT.2017.2680469

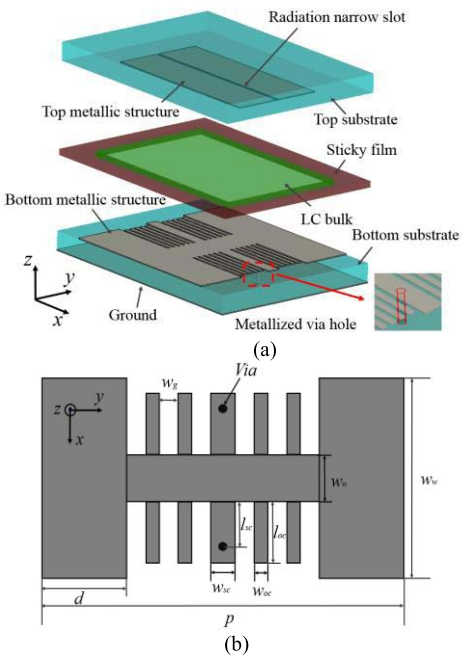

Fig. 1. (a) Geometry of the proposed unit cell. (b) Schematic of the bottom metallic structure.

In this paper, a design methodology for electrically controllable LC-CRLH-LWAs with large beam-steering range in printed circuit board (PCB) technology is proposed. Through mathematical analysis, it is proven that the balanced condition is well kept as the LC permittivity varied. Methods for enlarging the beam-steering range and bandwidth are subsequently proposed based on the analysis. A prototype is simulated, optimized, and experimentally tested to validate the design method. Results show that simulation and experimental data are in good agreement. An efficient method for the suppression of sidelobe levels (SLLs) is also discussed by eliminating the reflected wave between the unit cells of the antenna. The SLL is thus reduced from −5.1 to −8.2 dB.

II. Design Method Description

A. Antenna Structure Description

Similar to the conventional LWAs, an LC-CRLH-LWA is constructed by periodically cascading its unit cells [42]–[47]. The proposed unit cell structure of the LC-CRLH-LWA is depicted in Fig. 1(a). It is a kind of sandwich structure composed of three layers. The top layer and the bottom layer are dielectric substrates each carrying an etched metallic structure, whereas the bottom substrate contains an additional ground plane. The LC material is injected between the top metallic structure and bottom metallic structure and sealed with a sticky film. The sticky film is kept aloof from the metal structure to minimize its interference with the dominant RF field distribution within the multilayer topology. The lower surfaces of the top metallic structure and the upper surface of the bottom metallic structure are coated with polyvinyl alcohol, and the coatings of polyvinyl alcohol are rubbed to make LC director alignment along the y-direction.

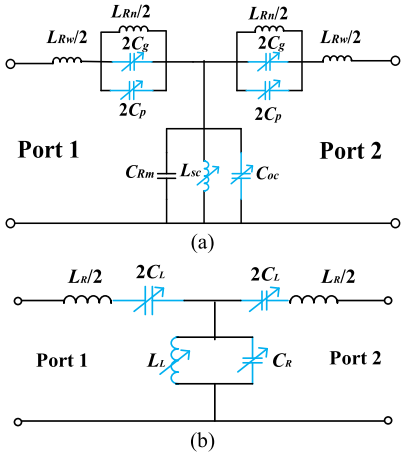

Fig. 2. (a) T-type equivalent network of the proposed LC-CRLH-LWA unit cell where the tunable elements are marked with blue. (b) Simplified T-type equivalent network of the proposed LC-CRLH-LWA unit cell.

The detailed drawing of the etched metallic structure on the bottom substrate layer is presented in Fig. 1(b). The bottom metallic structure can be considered as a modified version of microstrip line (MSL) topology (L_{Rw}, L_{Rn}, and C_{Rm}), where the central section of the MSL is narrowed down. Several stubs with lengths below a quarter guided wavelength are inserted to the narrowed MSL section. One pair of these stubs is short-circuited with metalized via holes, thus it behaves as an additional shunt inductance (L_{sc}) to the MSL. The rest of these stubs are open-circuited and serve as an additional shunt capacitance (C_{oc}). The gaps between the stubs perform as an additional series capacitance (C_g) in the MSL. The etched metallic structure on the lower surface of the top dielectric layer is a rectangular patch with a narrow slot. Hence, an additional series capacitance (C_p) emerges between the top metallic structure and the bottom metallic structure. The narrow slot in the top metallic structure supports leakage of electromagnetic waves to realize the antenna radiation.

In Fig. 2(a), the T-type equivalent network of the unit cell is reported, where no resistive elements are present. In the equivalent network, the narrow section of MSL is described as a parallel resonant circuit composed by L_{Rn}, C_g, and C_p. Through decreasing width of the narrowed MSL section with respect to the operation frequency, the parallel resonant circuit is designed to perform as an effective series capacitance. Therefore, the equivalent network of the unit cell is simplified as shown in Fig. 2(b). The relationship between the elements of the two T-type equivalent networks [see Fig. 2(a) and (b)] is given by

$$\begin{cases} C_L = C_p + C_g - 1/\omega^2 L_{\mathrm{Rn}} \\ C_R = C_{\mathrm{Rm}} + C_{\mathrm{oc}} \\ L_L = L_{\mathrm{sc}} \\ L_R = L_{\mathrm{Rw}} \end{cases} \tag{1}$$

where ω is the angular frequency, and C_L, C_R, L_L, and L_R can be explained as the effective distributed left-handed series capacitance, right-handed shunt capacitance, left-handed

shunt inductance, and right-handed series inductance of a corresponding CRLH unit cell, respectively [48]–[54].

B. Tunable Distributed Parameters

The LC material is locally uniaxial and homogeneous and presents macroscopically two permittivities: $\varepsilon_{//}$ (in the direction of the axes) and $\varepsilon_{\perp}$ (in the directions orthogonal to the axes) [55]. Usually, $\varepsilon_{//}$ is larger than $\varepsilon_{\perp}$ in microwave region. Referring to the Cartesian coodinate shown in Fig. 1(a), when there is no bias voltage applied, the LC director alignment is induced only with the rubbed coatings of polyvinyl alcohol, and then the permittivity tensor of the LC material (on its unbiased state) is exhibited as

$$\boldsymbol{\varepsilon}_{\mathrm{US}} = \left[\varepsilon_x, \varepsilon_y, \varepsilon_z\right] = \left[\varepsilon_{\perp}, \varepsilon_{//}, \varepsilon_{\perp}\right]. \tag{2}$$

If a 1-kHz bias voltage is applied between the top and bottom metallic structures, where the electric field's strength was considerably higher than the threshold of the transition for the duration of its application, the LC director alignment is produced with the bias voltage, and the permittivity tensor of the LC material (on its biased state) changes to

$$\boldsymbol{\varepsilon}_{\mathrm{BS}} = \left[\varepsilon_x, \varepsilon_y, \varepsilon_z\right] = \left[\varepsilon_{\perp}, \varepsilon_{\perp}, \varepsilon_{//}\right]. \tag{3}$$

In the proposed CRLH unit cell, the capacitances C_g, C_p, and C_{oc} and the inductance L_{sc} are adjacent to the tunable LC material (see Fig. 1), and hence these elements (marked with blue in Fig. 2) are steerable with LC permittivity. Among these tunable elements, the C_p can be approximately considered as a parallel-plate capacitor filled with the LC material, thus C_p is expressed with

$$C_p = \varepsilon_z S_{\mathrm{eff}} / h \tag{4}$$

where ε_z is the z-axis component of the LC permittivity tensor, S_{eff} is the effective area of the parallel plate capacitor, and h is the thickness of the LC layer. According to (2) and (3), when the LC permittivity varies from $\varepsilon_{\mathrm{US}}$ to $\varepsilon_{\mathrm{BS}}$, ε_z increases from $\varepsilon_{\perp}$ to $\varepsilon_{//}$. Thus, according to (4), C_p increases as the LC permittivity is tuned.

Referring to the Cartesian coodinate shown in Fig. 1(a), the capacitances C_g are mainly determined by the y-axis component of the LC permittivity tensor ε_y. According to (2) and (3), when the LC permittivity varies from $\varepsilon_{\mathrm{US}}$ to $\varepsilon_{\mathrm{BS}}$, ε_y decreases from $\varepsilon_{//}$ to $\varepsilon_{\perp}$ and leads to the diminution of C_g. Consequently, C_p and C_g vary in the opposite direction as the LC permittivity is tuned. As a result, the tunability of the total capacitance composed by C_p and C_g decreases because of the compensating effect of the C_p and C_g. In order to avoid the tunability degradation of the total capacitance, on one hand, the capacitance C_p is enlarged by decreasing the thickness of the LC layer. On the other hand, the capacitance C_g is greatly reduced by increasing the width of the gaps, and hence the C_g can be neglected. As shown in Fig. 3, the simulated electric field distribution is mainly directed along the z-axis, which proves that the capacitance C_p is the dominated capacitance.

The capacitance C_{oc} and inductance L_{sc} generated by the open-circuited stubs and short-circuited stubs, respectively, are

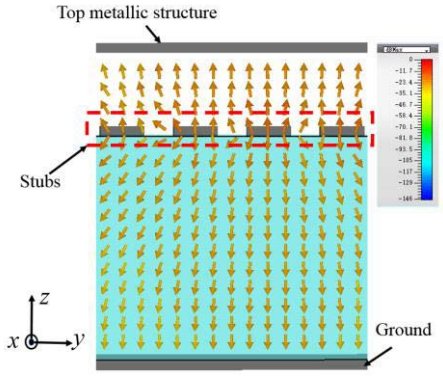

Fig. 3. Simulated local electric field distribution.

expressed by

$$C_{\mathrm{oc}} = \frac{\tan \beta_{\mathrm{oc}} l_{\mathrm{oc}}}{Z_{\mathrm{oc}} \omega} \tag{5a}$$

$$L_{\mathrm{sc}} = \frac{Z_{\mathrm{sc}} \tan \beta_{\mathrm{sc}} l_{\mathrm{sc}}}{\omega} \tag{5b}$$

where l_{oc} and l_{sc} are the length of open-circuited stubs and short-circuited stubs, respectively. β_{oc} and β_{sc} are the effective phase constants of the TLs corresponding to the open-circuited stubs and short-circuited stubs, respectively. Z_{oc} and Z_{sc} are the of the characteristic impedance of the two stub-TLs, respectively. In order to simplify the analysis, we assume that the the two stub-TLs have the same linewidth, and as a result, the two stub-TLs share the common effective permittivity $\varepsilon_{\mathrm{eff}}$ and characteristic impedance. In this case

$$\beta_{\mathrm{oc}} = \beta_{\mathrm{sc}} = \beta_s = \omega \sqrt{\varepsilon_{\mathrm{eff}}} / c \tag{6}$$

$$Z_{\mathrm{oc}} = Z_{\mathrm{sc}} = Z_s = \sqrt{L_{R,s} / C_{R,s}} \tag{7}$$

where c is the speed of light in vacuum, $L_{R,s}$ and $C_{R,s}$ are the common distributed parameters of the stub-TLs.

As shown in Fig. 3, the eletric field around the stubs is mainly directed along the z-axis, thus the $\varepsilon_{\mathrm{eff}}$ is mainly determined by the z-component ε_z of the LC permittivity tensor, and the variation of ε_z will cause the change of $\varepsilon_{\mathrm{eff}}$. The tunability of ε_z and the induced tunability of $\varepsilon_{\mathrm{eff}}$ are presented as

$$\eta_{\varepsilon_z} = (\varepsilon_{//} - \varepsilon_{\perp}) / \varepsilon_{\perp} \tag{8a}$$

$$\eta_{\varepsilon_{\mathrm{eff}}} = (\varepsilon_{\mathrm{eff,BS}} - \varepsilon_{\mathrm{eff,US}}) / \varepsilon_{\mathrm{eff,US}} \tag{8b}$$

where $\varepsilon_{\mathrm{eff,US}}$ and $\varepsilon_{\mathrm{eff,BS}}$ are the effective permittivity of the stub-TLs with LC material on its unbiased and biased state, respectively. Generally, $\eta_{\varepsilon z} > \eta_{\varepsilon \mathrm{eff}} > 0$.

According to (6) and (8), as the LC material is tuned from its unbiased state to its biased state, the phase constant β_s of the stub-TLs varies from

$$\beta_{s,\mathrm{US}} = \omega \sqrt{\varepsilon_{\mathrm{eff,US}}} / c \tag{9a}$$

$$\beta_{s,\mathrm{BS}} = \omega \sqrt{\varepsilon_{\mathrm{eff,BS}}} / c = \beta_{s,\mathrm{US}} \sqrt{1 + \eta_{\varepsilon_{\mathrm{eff}}}}. \tag{9b}$$

Based on the TL theory, the distributed shunt capacitance $C_{R,s}$ of the stub-TLs is proportional to $\varepsilon_{\mathrm{eff}}$, while the distributed series inductance $L_{R,s}$ is independent with $\varepsilon_{\mathrm{eff}}$.

Therefore, according to (7) and (8), as the LC permittivity is tuned, Z_s changes from

$$Z_{s,\mathrm{US}} = \sqrt{L_{R,s,\mathrm{US}}/C_{R,s,\mathrm{US}}} \tag{10a}$$

$$Z_{sc,\mathrm{BS}} = \sqrt{\frac{L_{R,s,\mathrm{US}}}{(1+\eta_{\varepsilon_{\mathrm{eff}}})C_{R,s,\mathrm{US}}}} = \frac{Z_{s,\mathrm{US}}}{\sqrt{1+\eta_{\varepsilon_{\mathrm{eff}}}}}. \tag{10b}$$

According to (5)–(10), capcitance C_{oc} and inductance L_{sc} are steered from the following equations with LC permittivity variation:

$$L_{sc,\mathrm{US}} = \frac{Z_{s,\mathrm{US}} \tan\beta_{s,\mathrm{US}} l_{\mathrm{sc}}}{\omega} \tag{11a}$$

$$C_{oc,\mathrm{US}} = \frac{\tan\beta_{s,\mathrm{US}} l_{\mathrm{oc}}}{Z_{s,\mathrm{US}}\omega} \tag{11b}$$

$$L_{sc,\mathrm{BS}} = \frac{Z_{s,\mathrm{US}} \tan(\beta_{s,\mathrm{US}} l_{\mathrm{sc}}\sqrt{1+\eta_{\varepsilon_{\mathrm{eff}}}})}{\omega\sqrt{1+\eta_{\varepsilon_{\mathrm{eff}}}}} \tag{11c}$$

$$C_{oc,\mathrm{BS}} = \frac{\sqrt{1+\eta_{\varepsilon_{\mathrm{eff}}}} \tan(\beta_{s,\mathrm{US}} l_{\mathrm{oc}}\sqrt{1+\eta_{\varepsilon_{\mathrm{eff}}}})}{Z_{s,\mathrm{US}}\omega}. \tag{11d}$$

Since $\eta_{\varepsilon\mathrm{eff}} > 0$, according to (11), C_{oc} and L_{os} increases as the LC permittivity is tuned.

According to (1), (4), and (11), the distributed parameters in (1) are tuned from the following equations, as the LC permittivity varied:

$$\begin{cases} C_{L,\mathrm{US}} = \varepsilon_\perp S_{\mathrm{eff}}/h - 1/\omega^2 L_{\mathrm{Rn}} \\ C_{R,\mathrm{US}} = C_{\mathrm{Rm}} + \dfrac{\tan\beta_{s,\mathrm{US}} l_{\mathrm{oc}}}{Z_{s,\mathrm{US}}\omega} \\ L_{L,\mathrm{US}} = \dfrac{Z_{s,\mathrm{US}} \tan\beta_{s,\mathrm{US}} l_{\mathrm{sc}}}{\omega} \\ L_{R,\mathrm{US}} = L_{\mathrm{Rw}} \end{cases} \tag{12a}$$

$$\begin{cases} C_{L,\mathrm{BS}} = (1+\eta_{\varepsilon_z})\varepsilon_\perp S_{\mathrm{eff}}/h - 1/\omega^2 L_{\mathrm{Rn}} \\ C_{R,\mathrm{BS}} = C_{\mathrm{Rm}} + \dfrac{\sqrt{1+\eta_{\varepsilon_{\mathrm{eff}}}} \tan(\beta_{s,\mathrm{US}} l_{\mathrm{oc}}\sqrt{1+\eta_{\varepsilon_{\mathrm{eff}}}})}{Z_{s,\mathrm{US}}\omega} \\ L_{L,\mathrm{BS}} = \dfrac{Z_{s,\mathrm{US}} \tan(\beta_{s,\mathrm{US}} l_{\mathrm{sc}}\sqrt{1+\eta_{\varepsilon_{\mathrm{eff}}}})}{\omega\sqrt{1+\eta_{\varepsilon_{\mathrm{eff}}}}} \\ L_{R,\mathrm{BS}} = L_{\mathrm{Rw}}. \end{cases} \tag{12b}$$

C. Realization of Large Beam-Steering Range

In a CRLH unit cell, both the series elements and shunt elements form a resonance circuit, respectively. A balanced condition can be achieved when the two circuits resonate at the same frequency. The balanced condition is expressed as

$$\omega_{se} = 1\sqrt{L_R C_L} = 11/\sqrt{L_L C_R}\omega_{sh} \tag{13}$$

where ω_{se} and ω_{sh} are the resonance angular frequencies of the series resonance circuit and shunt resonance circuit, respectively. For a broadside radiating LWA based on the balanced CRLH unit cell, the radiation angle θ is determined by

$$\theta = \sin^{-1}(\beta/k_0) \tag{14}$$

with β as the phase constant of the balanced CRLH unit cell, and k_0 is the wavenumber in free space. The phase constant β of the balanced CRLH unit cell is expressed as

$$\beta = \omega\sqrt{L_R C_R} - 1/\omega\sqrt{L_L C_L}. \tag{15}$$

As indicated by (15), the phase constant varies from negative to positive values with frequency. Thus, the CRLH LWA scans from backfire to endfire according to (14).

For an LC-CRLH-LWA, the radiation direction-frequency (θ-ω) curve displays a beam-steering range between two typical operating states, namely, the unbiased state and the biased state [14], [19]–[23]. The beam-steering range $\Delta\theta$ is obtained by

$$\Delta\theta = \theta_{\mathrm{BS}} - \theta_{\mathrm{US}} = \sin^{-1}(\beta_{\mathrm{BS}}/k_0) - \sin^{-1}(\beta_{\mathrm{US}}/k_0) \tag{16}$$

where θ_{US} and θ_{BS} are the radiation directions of the LC-CRLH-LWA for the two typical states, and θ_{US} and θ_{BS} are the associated phase constants of the LC-CRLH-TL. Since the inverse sine function is a monotonically increasing function, in order to achieve a wider range of beam steering $\Delta\theta$, a larger variation of the phase constant $\Delta\beta$ with respect to the two typical operating states is required. $\Delta\beta$ at the operation frequency ω_0 is obtained by

$$\begin{aligned} \Delta\beta &= \beta_{\mathrm{BS}} - \beta_{\mathrm{US}} \\ &= \omega_0\sqrt{L_{R,\mathrm{US}}C_{R,\mathrm{US}}}\left(\sqrt{\left(1+\frac{\Delta L_R}{L_{R,\mathrm{US}}}\right)\left(1+\frac{\Delta C_R}{C_{R,\mathrm{US}}}\right)}-1\right) \\ &\quad + \frac{1-\dfrac{1}{\sqrt{\left(1+\frac{\Delta L_L}{L_{L,\mathrm{US}}}\right)\left(1+\frac{\Delta C_L}{C_{L,\mathrm{US}}}\right)}}}{\omega_0\sqrt{L_{L,\mathrm{US}}C_{L,\mathrm{US}}}} \end{aligned} \tag{17}$$

where ΔC_L, ΔC_R, ΔL_L, and ΔL_R are the variation of C_L, C_R, L_L, and L_R, respectively.

According to (17), $\Delta\beta$ can be enlarged in two ways. The first way is increasing $C_R \times L_R$ and reducing $C_L \times L_L$. In the last section, in order to achieve a large tunability of the total capacitance composed by C_p and C_g, a small thickness of LC material h is necessary, which leads to a large C_L according to (12). In this case, in order to maintain the series resonance frequency ω_{se}, a relative smaller L_R is required. Therefore, a wide MSL with width w_w is selected to achieve a small L_{Rw}. Meanwhile, the wider MSL will generate a larger C_{Rm}, which help for the enhancement of C_R. In addition, the open-circuited stubs are introduced to enlarge C_R according to (12). Furthermore, in order to realize a larger C_R, the length of the open-circuited stubs l_{oc} is increased and multiple pairs of short-circuited stubs connected in parallel style are adopted. At the same time, in order to maintain a suitable shunt resonance frequency ω_{sh}, the length of the short-circuited stubs l_{sc} is reduced to provide a smaller L_L according to (12).

The more general way for increasing $\Delta\beta$ is to enhance the tunability of the distributed parameters. In the proposed LC-CRLH-LWA, C_L, C_R, and L_L are steerable, and according to (12), the tunability of each parameter is given by

$$\frac{\Delta C_L}{C_{L,\mathrm{US}}} = \frac{\eta_{\varepsilon_z}\varepsilon_\perp S_{\mathrm{eff}}/h}{\varepsilon_\perp S_{\mathrm{eff}}/h - 1/\omega^2 L_{R2}} \tag{18a}$$

$$\frac{\Delta C_R}{C_{R,\mathrm{US}}} = \frac{\sqrt{1+\eta_{\varepsilon_{\mathrm{eff}}}} \tan(\beta_{s,\mathrm{US}} l_{\mathrm{oc}}\sqrt{1+\eta_{\varepsilon_{\mathrm{eff}}}}) - \tan\beta_{s,\mathrm{US}} l_{\mathrm{oc}}}{Z_{s,\mathrm{US}}\omega(C_{R1}+C_{R2}) + \tan\beta_{s,\mathrm{US}} l_{\mathrm{oc}}} \tag{18b}$$

$$\frac{\Delta L_L}{L_{L,\mathrm{US}}} = \frac{\tan(\beta_{s,\mathrm{US}} l_{\mathrm{sc}}\sqrt{1+\eta_{\varepsilon_{\mathrm{eff}}}})}{\sqrt{1+\eta_{\varepsilon_{\mathrm{eff}}}} \tan\beta_{s,\mathrm{US}} l_{\mathrm{sc}}} - 1. \tag{18c}$$

Generally, LC material with a larger tunability results in a larger beam-steering range. Nevertheless, the LC tunability is usually limited by practical material engineering technology. According to (18a), increasing h and decreasing L_{R2} will improve the tunability of C_L. However, in order to maintain a dominated C_p compared to C_g, the enhancement of h is not desired. Hence, the beam-steering range can be enhanced by amplifying w_n. According to (18b) and (18c), increasing the length of the stubs $l_{\rm oc}$ and $l_{\rm sc}$ will enhance the tunability of L_L and C_R. Among them, according to (12), the increase of $l_{\rm sc}$ leads to the undesired enhancement of L_L, thus the value of $l_{\rm sc}$ should be selected under carefully weighing. Meanwhile, the increase of the length of the open-circuited stubs $l_{\rm oc}$ will result in the demanded amplification of C_R, thus in order to obtain a greater beam-steering range, a large $l_{\rm oc}$ (which is below a quarter guided wavelength) is required.

D. Steady Balanced Condition

Generally, the balanced condition of the LC-CRLH-LWAs tends to be broken as the LC permittivity varies, which results in the deterioration of the broadside radiation performance and the corresponding return loss during the backward-to-forward beam steering. In this section, the steady balanced condition of the proposed LC-CRLH-LWA is discussed.

As a precondition, we assume the balanced condition of the proposed LC-CRLH-LWA is achieved with LC material on its unbiased state. Thus, according to (12a) and (13), the balanced condition with LC material on its unbiased state is expressed with (19a). As the LC material is tuned to its biased state, in order to maintain the balanced condition, (13) should be satisfied too with the tuned distributed parameters given by (12b). In other words, (19b) should be satisfied

$$L_{\rm Rw}(\varepsilon_\perp S_{\rm eff}/h - 1/\omega^2 L_{\rm Rn}) = \frac{Z_{s,\rm US}\tan\beta_{s,\rm US}l_{\rm sc}}{\omega}\left(C_{\rm Rm} + \frac{\tan\beta_{s,\rm US}l_{\rm oc}}{Z_{s,\rm US}\omega}\right) \tag{19a}$$

$$L_{\rm Rw}[(1+\eta_{\varepsilon_z})\varepsilon_\perp S_{\rm eff}/h - 1/\omega^2 L_{\rm Rn}] = \frac{Z_{s,\rm US}\tan(\beta_{s,\rm US}l_{\rm sc}\sqrt{1+\eta_{\varepsilon_{\rm eff}}})}{\omega\sqrt{1+\eta_{\varepsilon_{\rm eff}}}} \times\left[C_{\rm Rm} + \frac{\sqrt{1+\eta_{\varepsilon_{\rm eff}}}\tan(\beta_{s,\rm US}l_{\rm oc}\sqrt{1+\eta_{\varepsilon_{\rm eff}}})}{Z_{s,\rm US}\omega}\right]. \tag{19b}$$

According to (19), the balanced condition of the proposed LC-CRLH-LWA is abstracted as a mathematical function

$$f(x) - g(y) = 0. \tag{20}$$

The functions $f(x)$ and $g(y)$ are expressed with (21a) and (21b), shown at the bottom of this page, respectively, where $x = \varepsilon_z/\varepsilon_\perp$ and $y = \varepsilon_{\rm eff}/\varepsilon_{\rm eff,US}$. When $x = y = 1$, (20) is corresponding to the balanced condition (19a) with LC material on its unbiased state, while as $x = 1 + \eta_{\varepsilon_z}$ and $y = 1 + \eta_{\varepsilon_{\rm eff}}$, (20) is corresponding to the balanced condition (19b) with LC material on its biased state. Since the balanced condition of the proposed LC-CRLH-LWA is achieved when the LC is on its unbiased state, (20) is satisfied when $x = y = 1$. Since $\eta_{\varepsilon_z} > \eta_{\varepsilon_{\rm eff}} > 0$, in order to enable (19b) to be satisfied, the derivative of $f(x)$ should be smaller than that of $g(y)$. The derivatives of $f(x)$ and $g(y)$ are given in (22a) and (22b) at the bottom of this page, where $f'(x)$ is a positive constant with fixed structure dimensions, while the $g'(y)$ is a monotonically increasing function in its domain of definition. Thus, when $f'(1) < g'(1)$ is achieved, the $f'(x) < g'(y)$ is satisfied on whole tuning range of LC permittivity. $f'(1) - g'(1)$ is expressed by (23) at the bottom of this page. As shown in (23), $f'(1) - g'(1)$ is the summation of three parts. In detail, the first part

$$\frac{C_{\rm Rm}Z_{s,\rm US}}{\omega}\left[\frac{3\sin(2\beta_{s,\rm US}l_{\rm sc}) - 2\beta_{s,\rm US}l_{\rm sc}}{4\cos^2(\beta_{s,\rm US}l_{\rm sc})}\right] \tag{24}$$

is negative when the length of the short-circuited stubs $l_{\rm sc}$ is larger than 0.18 times of guided wavelength, the second part

$$\frac{L_{\rm Rw}}{\omega^2 L_{\rm Rn}} \tag{25}$$

$$f(x) = \left[\frac{Z_{s,\rm US}\tan\beta_{s,\rm US}l_{\rm sc}}{\omega}(C_{\rm Rm} + \frac{\tan\beta_{s,\rm US}l_{\rm oc}}{Z_{s,\rm US}\omega})\right]x + \frac{(x-1)L_{\rm Rw}}{\omega^2 L_{\rm Rn}}, \quad x \in [1, 1+\eta_{\varepsilon_z}] \tag{21a}$$

$$g(y) = \frac{Z_{s,\rm US}\tan(\beta_{s,\rm US}l_{\rm sc}\sqrt{y})}{\omega\sqrt{y}}\left[C_{\rm Rm} + \frac{\sqrt{y}\tan(\beta_{s,\rm US}l_{\rm oc}\sqrt{y})}{Z_{s,\rm US}\omega}\right], \quad y \in [1, 1+\eta_{\varepsilon_{\rm eff}}] \tag{21b}$$

$$f'(x) = \frac{C_{\rm Rm}Z_{s,\rm US}}{\omega}\tan\beta_{s,\rm US}l_{\rm sc} + \frac{1}{\omega^2}\tan\beta_{s,\rm US}l_{\rm sc}\tan\beta_{s,\rm US}l_{\rm oc} + \frac{L_{\rm Rw}}{\omega^2 L_{\rm Rn}}, \quad x \in [1, 1+\eta_{\varepsilon_z}] \tag{22a}$$

$$g'(y) = \frac{C_{\rm Rm}Z_{s,\rm US}}{\omega}\frac{2\beta_{s,\rm US}l_{\rm sc}\sqrt{y} - \sin(2\beta_{s,\rm US}l_{\rm sc}\sqrt{y})}{4y^{\frac{3}{2}}\cos^2(\beta_{s,\rm US}l_{\rm sc}\sqrt{y})} + \frac{1}{\omega^2}\left[\frac{\beta_{s,\rm US}l_{\rm sc}\sin(2\beta_{s,\rm US}l_{\rm oc}\sqrt{y}) + \beta_{s,\rm US}l_{\rm oc}\sin(2\beta_{s,\rm US}l_{\rm sc}\sqrt{y})}{4\sqrt{y}\cos^2(\beta_{s,\rm US}l_{\rm sc}\sqrt{y})\cos^2(\beta_{s,\rm US}l_{\rm oc}\sqrt{y})}\right], \quad y \in [1, 1+\eta_{\varepsilon_{\rm eff}}] \tag{22b}$$

$$f'(1) - g'(1) = \frac{C_{\rm Rm}Z_{s,\rm US}}{\omega}\left[\frac{3\sin(2\beta_{s,\rm US}l_{\rm sc}) - 2\beta_{s,\rm US}l_{\rm sc}}{4\cos^2(\beta_{s,\rm US}l_{\rm sc})}\right] + \frac{L_{\rm Rw}}{\omega^2 L_{\rm Rn}} + \frac{1}{\omega^2}\left\{\frac{[\sin(2\beta_{s,\rm US}l_{\rm sc}) - 2\beta_{s,\rm US}l_{\rm sc}]\sin(2\beta_{s,\rm US}l_{\rm oc}) + [\sin(2\beta_{s,\rm US}l_{\rm oc}) - 2\beta_{s,\rm US}l_{\rm oc}]\sin(2\beta_{s,\rm US}l_{\rm sc})}{8\cos^2(\beta_{s,\rm US}l_{\rm sc})\cos^2(\beta_{s,\rm US}l_{\rm oc})}\right\} \tag{23}$$

is a positive constant, the third part

$$\frac{1}{\omega^2}\left\{\frac{[\sin(2\beta_{s,\mathrm{US}}l_{\mathrm{sc}})-2\beta_{s,\mathrm{US}}l_{\mathrm{sc}}]\sin(2\beta_{s,\mathrm{US}}l_{\mathrm{oc}})}{8\cos^2(\beta_{s,\mathrm{US}}l_{\mathrm{sc}})\cos^2(\beta_{s,\mathrm{US}}l_{\mathrm{oc}})}+\frac{[\sin(2\beta_{s,\mathrm{US}}l_{\mathrm{oc}})-2\beta_{s,\mathrm{US}}l_{\mathrm{oc}}]\sin(2\beta_{s,\mathrm{US}}l_{\mathrm{sc}})}{8\cos^2(\beta_{s,\mathrm{US}}l_{\mathrm{sc}})\cos^2(\beta_{s,\mathrm{US}}l_{\mathrm{oc}})}\right\} \quad (26)$$

is negative, and it can be easily calculated that (26) monotonously decreases with the length of the two stubs l_{oc} and l_{sc}. According to (24)–(26), through tuning l_{oc} and l_{sc}, a negative (23) can be easily achieved. Therefore, $f'(x) < g'(y)$ is satisfied during the whole tuning range of LC permittivity. Furthermore, since the range of tangent function varies in $(0, +\infty)$ with function argument change in $(0, \pi/2)$, the value of $f'(x)-g'(y)$ can be steered in a large range through tuning l_{oc} and l_{sc} according to (22). Hence, with proper selection of dimension parameters, we can certainly enable (20) be satisfied when $x = 1 + \eta_{\varepsilon_z}$ and $y = 1 + \eta_{\varepsilon_{\mathrm{eff}}}$. That is, the balanced condition is satisfied with LC on its biased state.

In summary, the proposed unit cell presents the capability of keeping a steady balanced condition with varying LC permittivity through synchronously controlling the distributed series elements and shunt elements.

E. Achievement of Broadband Property

Broadband property of the LWA is the basis to realize an LC-LWA with a satisfied frequency band. In order to achieve the broadband property, the effective impedance of the CRLH unit cell should be stable in a wide frequency band. Based on the theory of the CRLH-TLs [52]–[54], the Bloch impedance Z_B of the CRLH-TL can be expressed by (27) at the bottom of this page. In order to achieve broadband property, the numerator and denominator of Z_B should vary with frequency harmonically. According to (27), Z_B is mainly determined by the inherent distributed parameters of the modified MSL and the shunt distributed parameters generated by the stubs. Among them, the inherent distributed parameters (L_{Rw}, L_{Rn}, and C_{Rm}) that are steered by the linewidths w_w and w_n affect both the numerator and denominator of Z_B; thus through tuning w_w and w_n, a roughly harmonic tuning of the numerator and denominator can be realized. Meanwhile, the shunt distributed parameters that are tuned by the lengths of stub l_{oc} and l_{sc} only influence the denominator. That is, the denominator can be controlled independently. Hence, the more harmonic variation between the numerator and denominator can be achieved by changing l_{oc} and l_{sc}. In other words, a stable Z_B that confirms the broadband property is realized.

III. Numerical Simulation of Prototype

A. Unit Cell Validation

In order to demonstrate the proposed design methodology for the LC-CRLH-LWAs, a prototype is designed, simulated, and tested. The antenna is designed to operate within the frequency range of 12.25–12.75 GHz, which includes the main downlink frequency for Ku-band satellite communication.

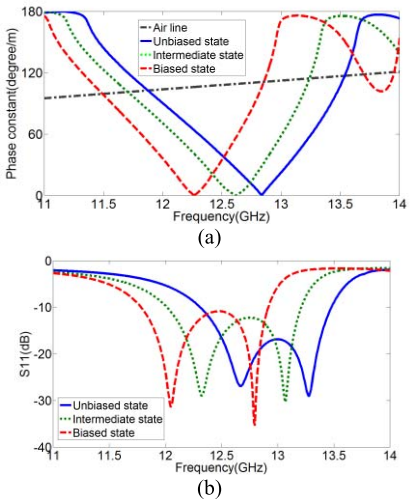

Fig. 4. (a) Dispersion curves of the proposed unit cell for different LC states. (b) S_{11} of the proposed unit cell for different LC states.

Two layers of Rogers RO4350B substrate with permittivity of 3.48, thickness of 0.762 mm, and dielectric loss tangent $\tan\delta = 0.004$ are chosen for the top and bottom substrate layers (see Fig. 1). To reduce the complexity of the fabrication, the width of the short-circuited stubs is intentionally increased. The detailed dimensions (in millimeters) are given as follows: $w_m = 7.4$, $w_n = 1.5$, $l = 2.75$, $S = 1.95$, $w_{\mathrm{sc}} = 0.5$, $w_{\mathrm{oc}} = 0.15$, $w_g = 0.1$, and $d = 2$. In our simulations, the LC GT3-23001, which is a commercial product of Merck KGaA, is applied. Its relative permittivity is alterable from 2.5 to 3.3 depending on the applied bias voltage. The thickness of LC layer is 0.25 mm. An intermediate state associated with full broadside radiation is linked to the intermediate permittivity value of 2.9 that is utilized as a starting point for the subsequent antenna design.

The numerical simulations of the dispersion diagram and the return loss of the unit cell are conducted using the computational electromagnetics simulation platform CST Microwave Studio, where the results are plotted in Fig. 4(a) and (b), respectively. It can be observed that the unit cell is balanced at 12.55 GHz when the LC is tuned to its intermediate state. Moreover, both the balanced condition and the impedance matching condition are well kept during the tuning of the LC permittivity. A relative wide bandwidth from 12 to 13.2 GHz for the intermediate state of the LC is achieved despite the quite steep slope of the β-ω curve.

B. Frequency Scanning Property of the LC-CRLH-LWA

An LC-CRLH-LWA can be easily obtained by periodically cascading the unit cells a finite number of times. In this

$$Z_B = \sqrt{\frac{j\omega L_R + 1/j\omega C_L}{j\omega C_R + 1/j\omega L_L}} = \sqrt{\frac{L_{\mathrm{Rw}}[C_p - (1/L_{\mathrm{Rn}} + 1/L_{\mathrm{Rw}})/\omega^2]}{(C_p - 1/\omega^2 L_{\mathrm{Rn}})[C_{\mathrm{Rm}} + \tan\beta_s l_{\mathrm{oc}}/Z_s\omega - 1/Z_s\omega\tan\beta_s l_{\mathrm{sc}}]}} \quad (27)$$

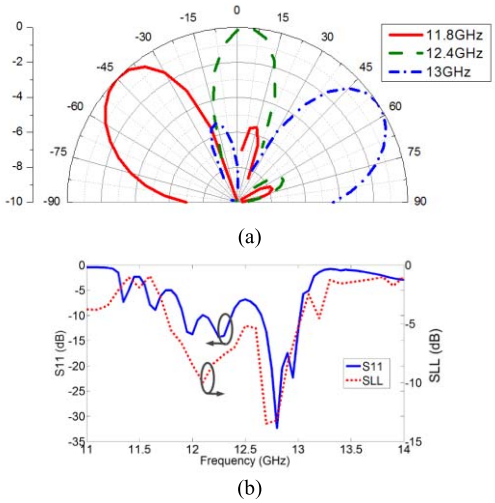

Fig. 5. (a) Simulated radiation patterns at different frequencies for the five-cell CRLH-LWA. (b) Simulated return loss and SLL of the five-cell CRLH-LWA with LC material on its intermediate state.

TABLE I
COMPARISON OF THE BEAM-SCANNING RANGE PER GIGAHERTZ

	[39]	[40]	[41]	This work
Beam scanning range (degree)	-22 ~ +34	-30 ~ +46	-46 ~ +40	-47 ~ +56
Frequency band (GHz)	12.5 ~ 16.5	9.5 ~ 12.4	8.6 ~ 10.3	11.8 ~ 13
Beam scanning range per GHz	14°	26.2°	50.6°	85.8°

section, the frequency scanning property of the proposed LC-CRLH-LWA is studied to provide a basis for the understanding of the electrical beam steering characteristics.

The simulated normalized E-plane radiation patterns of the LC-CRLH-LWA with five unit cells are presented in Fig. 5(a) for three different operation frequencies. The continuous free-space beam-scanning capability of this CRLH-LWA is clearly demonstrated. A scanning range from $-47°$ to $+59°$ is obtained for a frequency variation from 11.8 to 13 GHz. The frequency scanning property of our designed antenna is now compared to three recently proposed LWAs, where the comparison is displayed in Table I [39]–[41]. According to the table, the designed antenna obtains a wider frequency-tuned beam-scanning range and a much steeper slope of the θ-ω curve. The proposed antenna, operating as a frequency scanning LWA, is expected to have applications in radar and satellite communication systems, which require wide frequency-tuned beam scanning ranges and fast steering speeds.

The simulated return loss and SLL of the five-cell CRLH-LWA with LC material stick to its intermediate state are presented in Fig. 5(b), where the return loss of the proposed antenna gets worse compared to that of the unit cell. This phenomenon is produced by the superposition of spurious reflections emerging between the unit cells. The radiation performance of the antenna is further affected by this kind of worse return loss.

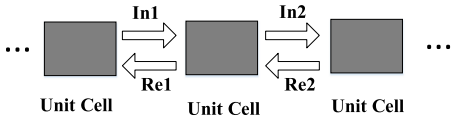

Fig. 6. Schematic of the reflection among the unit cells.

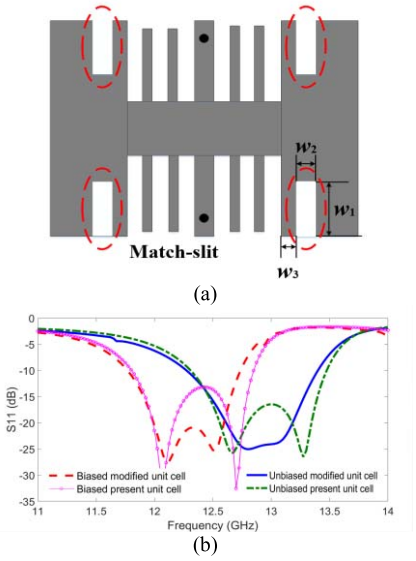

Fig. 7. (a) Geometry of the modified etched metallic structure on the bottom substrate layer with MS. (b) Return loss of the unit cell with and without MS for different LC states.

C. Efficient Method for SLL Suppression

SLL is a very important parameter for the radiation performance of any antenna. In case of LC-CRLH-LWAs, the SLL usually deteriorates as the permittivity of the LC is tuned. However, efficient methods to lower the SLL of the electromagnetic metamaterial-based LWAs are rarely discussed in the literature.

An LWA is generally considered as a traveling-wave antenna. However, residual reflections among the unit cells and between the feeding structure and the antenna are unavoidable in any practical LWA. The schematic of the reflections among the unit cells is presented in Fig. 6. These reflections form a distributed cohort of reversed traveling waves, which contribute to undesired radiation emission with directions deviating from the main beam direction. It is clearly revealed in Fig. 5(b) that lower return loss leads to lower SLLs, meaning that less reflections will result in lower SLLs too. Therefore, in order to decrease SLL of the proposed LC-CRLH-LWA, we concentrate on reflection suppression within the proposed LWA topology.

In order to minimize the reflections within the present LWA structure, additional matching-slits (MS) are proposed, as shown in Fig. 7(a). Through elaborately designing the dimension and position of the MS, the impedance matching between the unit cells is optimized. For comparison, the simulated return loss of the unit cell with and without the MS is plotted in Fig. 7(b). As shown in Fig. 7(b), the passband of the modified unit cell is considerably flattened around the

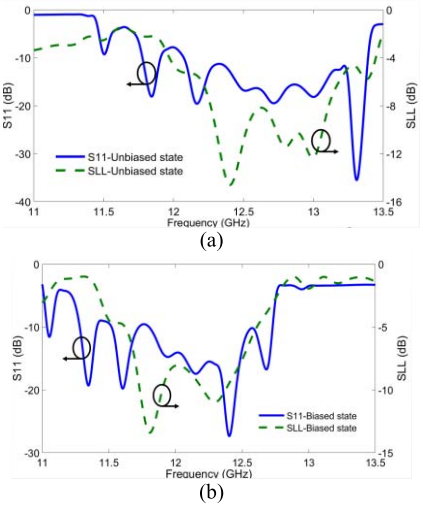

Fig. 8. (a) Simulated return loss and SLL of the modified five-cell LC-CRLH-LWA with LC material on its unbiased state. (b) Simulated return loss and SLL of the modified five-cell LC-CRLH-LWA with LC material on its biased state.

balanced frequency, yielding a reduction of the return loss of more than 5.3 dB for all LC states compared. Fig. 8 depicts the simulated return loss and SLL of the modified five-cell LC-CRLH-LWA for different LC states. Since the reflections were suppressed, the peak magnitude of the SLL around the balanced frequency decreased from −5.1 to −8.2 dB. Benefiting from the wide bandwidth of the proposed unit cell, the LC-CRLH-LWA achieves a wide bandwidth with respect to the operation frequency. Simulated results show the return loss (for the intermediate state) is lower than −10 dB from 11.78 to 13.09 GHz, which covers the total frequency scanning band. For the whole steering range of the LC permittivity, the antenna presents a return loss lower than −10 dB in the range of 12.14–12.77 GHz, covering a band of 630 MHz, which coincides with the main downlink frequency range of Ku-band satellite communications.

In order to indicate the relationship between the return loss and SLL, the feature selective validation technique is applied [56]–[58]. As shown in Fig. 9(a), the point-by-point comparisons of the feature difference measure intensity (FDMi) between the return loss and SLL are presented for different LC states. For all LC states, the agreement between two data sets is good from 11.95 to 12.3 GHz and is nearly very good from 12.3 to 13.15 GHz, which covers the whole operating band of the proposed five-cell LC-CRLH-LWA. The grade-spread chart for the return loss and SLL from 11.95 to 12.3 GHz is exhibited in Fig. 9(b) with a threshold value of 85%. The grade starts with the excellent category and cumulates a total equal to threshold value as categories are added, while the spread starts with the highest category. As shown in Fig. 9(b), the grade and spread of feature difference measure for the unbiased state are both 3, which means excellent + very good + good > 85%, while the value is 2 for the biased state, which indicates that excellent + very good > 85%. In other words, the SLL agrees well with the return loss in the operating band. Hence, the proposed method of SLL suppression through reducing reflections is validated.

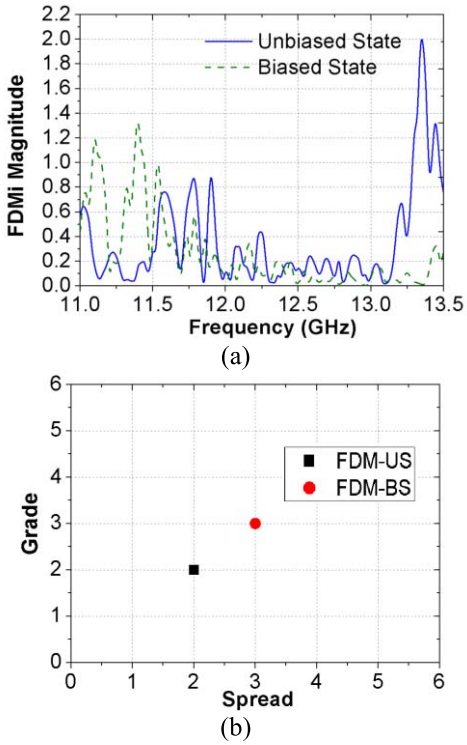

Fig. 9. (a) Point-by-point analysis of the feature difference (FDMi) between the return loss and SLL where the category ranges are excellent < 0.1, very good 0.1–0.2, good 0.2–0.4, fair 0.4–0.8, poor 0.8–1.6, and very poor > 1.6. (b) Grade-spread chart for the return loss and SLL.

D. Electrical Scanning of Radiation Beam

As depicted in Fig. 4, the dispersion curves of the proposed unit cell shift horizontally as the LC permittivity is tuned. In the meantime, the balanced condition and the impedance matching condition are well kept for different LC states. Thus, the proposed antenna is a very promising candidate for fixed-frequency beam-steering LWAs.

The complete five-cell LC-CRLH-LWA is formed by adding an impedance transformer that further optimizes the return loss and the associated SLL and a bias network for the applying of bias voltage. Fig. 10(a) presents the simulated spectral responses of the radiation angles of the LC-CRLH-LWA for three different LC states. The radiation angle varies from −21° to +23° at an operation frequency of 12.4 GHz for varying permittivity of the correspondingly biased LC material. Fig. 10(b) displays the radiation patterns at 12.4 GHz for the same three LC states, providing an SLL lower than −11.3 dB during the beam steering.

IV. Experimental Validation

For validation purposes, the designed five-cell LC-CRLH-LWA prototype was fabricated on PCB as depicted in Fig. 11(a). The LC material applied in the manufactured LWA is LC CDZSL-016 provided by the LuQuan Company, Ltd. The LC CDZSL-016 presents a permittivity varying from 2.7 to 3.25 when measured with the method proposed in [59]. Fig. 11(b) shows the measured scattering parameters versus bias voltages using an Agilent N5227A vector network

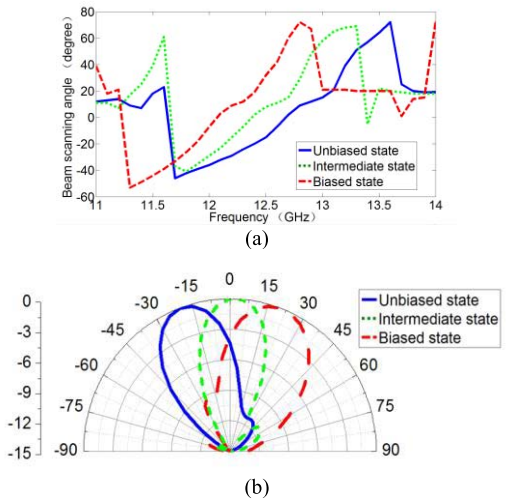

Fig. 10. (a) Simulated spectral responses of the radiation angles of the LC-CRLH-LWA for different LC states. (b) Beam steering property for different LC states at an operation frequency of 12.4 GHz.

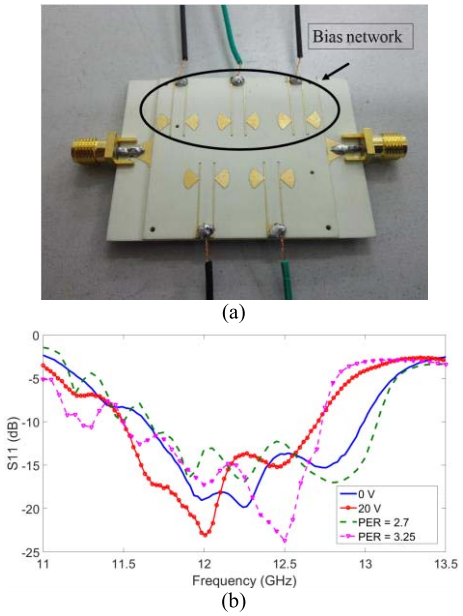

Fig. 11. (a) Photograph of the fabricated LC-CRLH-LWA. (b) Measured and simulated return loss of the antenna for the bias voltages 0 and 20 V associated with the corresponding permittivities (PER) 2.7 and 3.25, respectively.

analyzer. The measured return loss is lower than −10 dB between the two frequencies 11.83 and 12.72 GHz for the associated bias voltages of 0 and 20 V, respectively. The measured results (plotted as solid lines) agree well with the simulated data (plotted as dashed lines).

The measured frequency scanning of the radiation pattern for the unbiased state of the antenna is presented in Fig. 12(a). The direction of the main lobe starts at an angle of −54° and reaches an emission angle of +57° for an operation frequency ranging from 11.8 to 12.9 GHz. The E-plane radiation patterns are measured for different bias voltages at three different fixed operation frequencies to demonstrate the full capability of electrically controlled beam steering.

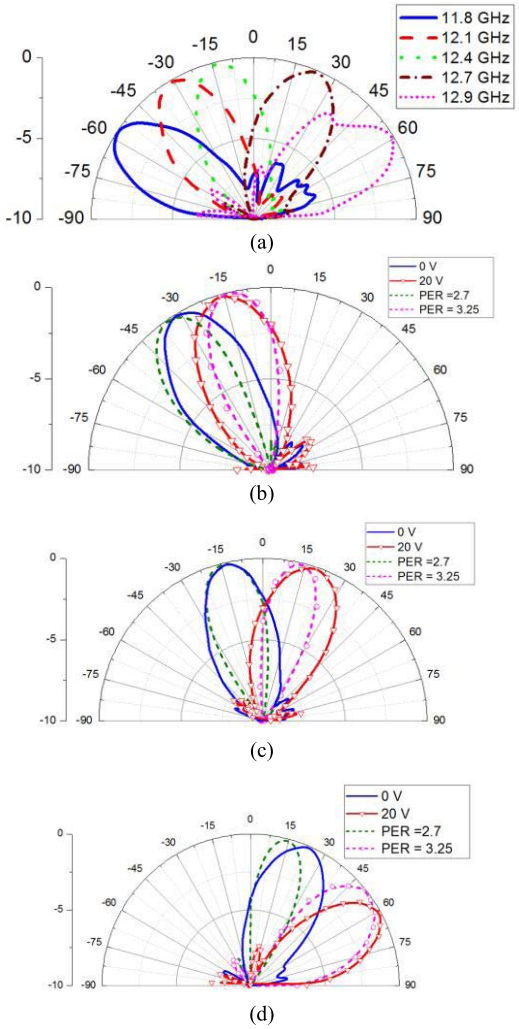

Fig. 12. Measured (solid line) and simulated (dashed lines) radiation pattern of the proposed LC-CRLH-LWA. (a) Measured frequency scanning from 11.8 to 12.9 GHz for the unbiased state. (b) Electrical beam steering at 12.1 GHz. (c) Electrical beam steering at 12.4 GHz. (d) Electrical beam steering at 12.7 GHz.

The normalized radiation patterns are given in Fig. 11(b)–(d). The measured main lobe directions are electrically steered from −32° to −16° at 12.1 GHz (backfire), from −13° to +18° at 12.4 GHz (broadside), and from +22° to +60° at 12.7 GHz (endfire). The simulated radiation patterns adopting the LC CDZSL-016 are plotted in Fig. 12(b)–(d) as dashed lines, showing a good agreement with the measured emission patterns (solid lines). Furthermore, it is observed that the ranges of electrical beam steering are wider for broadside and endfire radiation than for backfire radiation. This phenomenon agrees well with the simulation results.

V. Conclusion

A novel method for the designing of the fixed-frequency CRLH-LWA employing LC in PCB technology that supports a large beam-steering range, steady balanced condition, and broadband property has been proposed. It is mathematically demonstrated that the balanced condition of the unit cell and the resulting LWA are well kept as the permittivity of the LC is electrically tuned. Methods for the enhancement of

beam-steering range and broadband property are presented based on the theoretical analysis. A Ku-band LC-CRLH LWA prototype has been designed and optimized based on the proposed design method. The realized antenna presents a measured frequency scanning range from -54° to $+57^\circ$ for a frequency variation from 11.8 to 12.9 GHz. The overall exploitable bandwidth reaches from 11.65 to 13.05 GHz. It is revealed that the residual reflections among the unit cells cause a poor suppression of the SLL. Corresponding optimization for achieving lower SLLs in the radiation patterns has been successfully carried out by lowering the return loss for the unit cell. A large voltage-controlled scanning range of the radiation pattern has been achieved. The antenna exhibits a simulated beam-steering ranging from -21° to $+23^\circ$ at a fixed frequency of 12.4 GHz for broadside radiation, showing SLLs lower than -11.3 dB. The measured scanning range of electrically beam steering extends from -13° to $+18^\circ$. The proposed LC-CRLH-LWA is a valuable candidate and easy-to-fabricate antenna structure for radar and satellite communication system due to its low loss, low cost, low profile, and highly versatile scanning properties.

ACKNOWLEDGMENT

The authors would like to thank Prof. X. Gong from the University of Central Florida, Orlando, FL, USA, for the very fruitful comments and discussions.

REFERENCES

[1] L. Juhua, D. R. Jackson, and Y. Long, "Substrate integrated waveguide (SIW) leaky-wave antenna with transverse slots," *IEEE Trans. Antennas Propag.*, vol. 60, no. 1, pp. 20–29, Jan. 2012.

[2] F. Xu, K. Wu, and X. Zhang, "Periodic leaky-wave antenna for millimeter wave applications based on substrate integrated waveguide," *IEEE Trans. Antennas Propag.*, vol. 58, no. 2, pp. 340–347, Feb. 2010.

[3] A. J. Martinez-Ros, J. L. Gomez-Tornero, and G. Goussetis, "Planar leaky-wave antenna with flexible control of the complex propagation constant," *IEEE Trans. Antennas Propag.*, vol. 60, no. 3, pp. 1625–1630, Mar. 2012.

[4] J.-D. Park and A. M. Niknejad, "Y-band on-chip dual half-width leaky-wave antenna in a nanoscale CMOS process," *IEEE Antennas Wireless Propag. Lett.*, vol. 12, pp. 1476–1479, 2013.

[5] W. Hong, T.-L. Chen, C.-Y. Chang, J. W. Sheen, and Y.-D. Lin, "Broadband tapered microstrip leaky-wave antenna," *IEEE Trans. Antennas Propag.*, vol. 51, no. 8, pp. 1922–1928, Aug. 2003.

[6] Y. Li, Q. Xue, H.-Z. Tan, and Y. Long, "The half-width microstrip leaky wave antenna with the periodic short circuits," *IEEE Trans. Antennas Propag.*, vol. 59, no. 9, pp. 3421–3423, Sep. 2011.

[7] J. Liu, D. R. Jackson, Y. Li, C. Zhang, and Y. Long, "Investigations of SIW leaky-wave antenna for endfire-radiation with narrow beam and sidelobe suppression," *IEEE Trans. Antennas Propag.*, vol. 62, no. 9, pp. 4489–4497, Sep. 2014.

[8] Y. J. Cheng, Y. X. Guo, X. Y. Bao, and K. B. Ng, "Millimeter-wave low temperature co-fired ceramic leaky-wave antenna and array based on the substrate integrated image guide technology," *IEEE Trans. Antennas Propag.*, vol. 62, no. 2, pp. 669–676, Feb. 2014.

[9] N. Rihem, L. Lassaad, H. Hanen, and G. Ali, "New design of SIW leaky wave antenna based on a T-shaped slot with controllable scanning rate from backward to forward direction," in *Proc. IEEE 15th Mediterr. Microw. Symp.*, Dec. 2015, pp. 1–4.

[10] C.-J. Wang, Y.-C. Shih, and C. F. Jou, "Beam-switchable scanning leaky-wave antenna," *Electron. Lett.*, vol. 36, no. 7, pp. 596–597, Mar. 2000.

[11] R. E. Horn, H. Jacobs, E. Freibergs, and K. L. Klohn, "Electronic Modulated Beam-Steerable Silicon Waveguide Array Antenna," *IEEE Trans. Microw. Theory Techn.*, vol. MTT-28, no. 6, pp. 647–653, Jun. 1980.

[12] H. Maheri, M. Tsutsumi, and N. Kumagai, "Experimental studies of magnetically scannable leaky-wave antennas having a corrugated ferrite slab/dielectric layer structure," *IEEE Trans. Antennas Propag.*, vol. 36, no. 7, pp. 911–917, Jul. 1988.

[13] L. Huang, J.-C. Chiao, and M. P. D. Lisio, "An electronically switchable leaky wave antenna," *IEEE Trans. Antennas Propag.*, vol. 48, no. 11, pp. 1769–1772, Nov. 2000.

[14] S. Lim, C. Caloz, and T. Itoh, "Metamaterial-based electronically controlled transmission-line structure as a novel leaky-wave antenna with tunable radiation angle and beamwidth," *IEEE Trans. Microw. Theory Techn.*, vol. 52, no. 12, pp. 2678–2690, Dec. 2004.

[15] F. Jiahui, X. Li, Q. Wu, and C. Feng, "Metamaterial based electronically-scanned circularly-polarized LWA," *IEEE Trans. Magn.*, vol. 48, no. 11, pp. 4301–4304, Nov. 2012.

[16] N. Apaydin, K. Sertel, and J. L. Volakis, "Nonreciprocal and magnetically scanned leaky-wave antenna using coupled CRLH lines," *IEEE Trans. Antennas Propag.*, vol. 62, no. 6, pp. 2954–2961, Jun. 2014.

[17] J. A. Hejase, J. Myers, L. Kempel, and P. Chahal, "Design study of electronically steerable half-width microstrip leaky wave antennas," in *Proc. IEEE 61st Electron. Compon. Technol. Conf.*, Jun. 2011, pp. 1348–1353.

[18] K. Sato, S. Matsuzawa, Y. Inoue, and T. Nomura, "Electronically scanned left-handed leaky wave antenna for millimeter-wave automotive applications," in *Proc. IEEE Int. Workshop Antenna Technol. Small Antennas Novel Metamater.*, Mar. 2006, pp. 420–423.

[19] C. Damm, M. Maasch, R. Gonzalom, and R. Jakoby, "Tunable composite right/left-handed leaky wave antenna based on a rectangular waveguide using liquid crystals," in *IEEE MTT-S Int. Microw. Symp. Dig.*, May 2010, pp. 13–16.

[20] M. Roig, M. Maasch, C. Damm, and R. Jakoby, "Steerable Ka-Band leaky wave antenna based on liquid crystal material," in *Proc. 7th Int. Congr. Adv. Electromagn. Mater. Microw. Opt.*, Sep. 2013, pp. 540–545.

[21] M. Roig, M. Maasch, C. Damm, O. H. Karabey, and R. Jakoby, "Liquid crystal based tunable composite right/left-handed leaky-wave antenna for Ka-band applications," in *Proc. Eur. Microw. Conf.*, Oct. 2013, pp. 759–762.

[22] M. Roig, M. Maasch, C. Damm, and R. Jakoby, "Dynamic beam steering properties of an electrically tuned liquid crystal based CRLH leaky wave antenna," in *Proc. 8th Int. Congr. Adv. Electromagn. Mater. Microw. Opt.*, Aug. 2014, pp. 253–255.

[23] M. Roig, M. Maasch, C. Damm, and R. Jakoby, "Electrically tunable liquid crystal based composite right/left-handed leaky-wave antenna at 26.7 GHz," in *Proc. 44th Eur. Microw. Conf.*, Oct. 2014, pp. 331–334.

[24] M. Roig, M. Maasch, C. Damm, and R. Jakoby, "Investigation and application of a liquid crystal loaded varactor in a voltage tunable CRLH leaky-wave antenna at Ka-band," *Int. J. Microw. Wireless Technol.*, vol. 7, nos. 3–4, pp. 361–367, Jun. 2015.

[25] J.-C. S. Chieh and A.-V. Pham, "A bidirectional microstrip X-band antenna array on liquid crystal polymer for beamforming applications," *IEEE Trans. Antennas Propag.*, vol. 61, no. 6, pp. 3364–3368, Jun. 2013.

[26] O. H. Karabey, S. Bildik, S. Bausch, S. Strunck, A. Gaebler, and R. Jakoby, "Continuously polarization agile antenna by using liquid crystal-based tunable variable delay lines," *IEEE Trans. Antennas Propag.*, vol. 61, no. 1, pp. 70–76, Jan. 2013.

[27] O. H. Karabey, A. Mehmood, M. Ayluctarhan, H. Braun, M. Letz, and R. Jakoby, "Liquid crystal based phased array antenna with improved beam scanning capability," *Electron. Lett.*, vol. 50, no. 6, pp. 426–428, Mar. 2014.

[28] A. C. Polycarpou, M. A. Christou, and N. C. Papanicolaou, "Tunable patch antenna printed on a biased nematic liquid crystal cell," *IEEE Trans. Antennas Propag.*, vol. 62, no. 10, pp. 4980–4987, Oct. 2014.

[29] S. Bildik, S. Dieter, C. Fritzsch, W. Menzel, and R. Jakoby, "Reconfigurable folded reflectarray antenna based upon liquid crystal technology," *IEEE Trans. Antennas Propag.*, vol. 63, no. 1, pp. 122–132, Jan. 2015.

[30] N. Tentillier, F. Krasinski, R. Sauleau, B. Splingart, H. Lhermite, and P. Coquet, "A liquid-crystal, tunable, ultra-thin Fabry-Perot resonator in Ka band," *IEEE Antennas Wireless Propag. Lett.*, vol. 8, pp. 701–704, 2009.

[31] M. Yazdanpanahi, S. Bulja, D. Mirshekar-Syahkal, R. James, S. E. Day, and F. A. Fernandez, "Measurement of dielectric constants of nematic liquid crystals at mm-wave frequencies using patch resonator," *IEEE Trans. Instrum. Meas.*, vol. 59, no. 12, pp. 3079–3085, Dec. 2010.

[32] O. H. Karabey, S. Bausch, S. Bildik, S. Strunck, A. Gaebler, and R. Jakoby, "Design and application of a liquid crystal varactor based tunable coupled line for polarization agile antennas," in *Proc. 42nd Eur. Microw. Conf.*, Nov. 2012, pp. 413–416.

[33] G. Perez-Palomino *et al.*, "Design and experimental validation of liquid crystal-based reconfigurable reflectarray elements with improved bandwidth in F-band," *IEEE Trans. Antennas Propag.*, vol. 61, no. 4, pp. 1704–1713, Apr. 2013.
[34] N. C. Papanicolaou, M. A. Christou, and A. C. Polycarpou, "Frequency-agile microstrip patch antenna on a biased liquid crystal substrate," *Electron. Lett.*, vol. 51, no. 3, p. 202-U28, Feb. 2015.
[35] G. Perez-Palomino *et al.*, "Design and demonstration of an electronically scanned reflectarray antenna at 100 GHz using multiresonant cells based on liquid crystals," *IEEE Trans. Antennas Propag.*, vol. 63, no. 8, pp. 3722–3727, Aug. 2015.
[36] S. Strunck *et al.*, "Reliability study of a tunable Ka-band SIW-phase shifter based on liquid crystal in LTCC-technology," *Int. J. Microw. Wireless Technol.*, vol. 7, no. 5, pp. 521–527, Oct. 2015.
[37] S. Mueller *et al.*, "Broad-band microwave characterization of liquid crystals using a temperature-controlled coaxial transmission line," *IEEE Trans. Microw. Theory Techn.*, vol. 53, no. 6, pp. 1937–1945, Jun. 2005.
[38] F. Goelden *et al.*, "Tunable liquid crystal phase shifter for microwave frequencies," *Electron. Lett.*, vol. 45, no. 13, pp. 686–687, 2009.
[39] C. Jin and A. Alphones, "Leaky-wave radiation behavior from a double periodic composite right/left-handed substrate integrated waveguide," *IEEE Trans. Antennas Propag.*, vol. 60, no. 4, pp. 1727–1735, Apr. 2012.
[40] K. Dong-Jin and L. Jeong-Hae, "Beam scanning leaky-wave slot antenna using balanced CRLH waveguide operating above the cutoff frequency," *IEEE Trans. Antennas Propag.*, vol. 61, no. 5, pp. 2432–2440, May 2013.
[41] Q. Yang, X. Zhao, and Y. Zhang, "Composite right/left-handed ridge substrate integrated waveguide slot array antennas," *IEEE Trans. Antennas Propag.*, vol. 62, no. 4, pp. 2311–2316, Apr. 2014.
[42] S. Lim, C. Caloz, and T. Itoh, "A reflectodirective system using a composite right/left-handed (CRLH) leaky-wave antenna and heterodyne mixing," *IEEE Microw. Wireless Compon. Lett.*, vol. 14, no. 4, pp. 183–185, Apr. 2004.
[43] J. S. Gomez-Diaz, A. Alvarez-Melcon, and T. Bertuch, "A modal-based iterative circuit model for the analysis of CRLH leaky-wave antennas comprising periodically loaded PPW," *IEEE Trans. Antenna Propag.*, vol. 59, no. 4, pp. 1101–1112, Apr. 2011.
[44] T. Kodera, D. L. Sounas, and C. Caloz, "Nonreciprocal magnetless CRLH leaky-wave antenna based on a ring metamaterial structure," *IEEE Antennas Wireless Propag. Lett.*, vol. 10, pp. 1551–1554, 2011.
[45] R. Siragusa, E. Perret, P. Lemaitre-Auger, H. van Nguyen, S. Tedjini, and C. Caloz, "A tapered CRLH interdigital/stub leaky-wave antenna with minimized sidelobe levels," *IEEE Antennas Wireless Propag. Lett.*, vol. 11, pp. 1214–1217, 2012.
[46] Y.-J. Chi and F.-C. Chen, "CRLH leaky wave antenna based on ACPS technology with 180°C horizontal plane scanning capability," *IEEE Trans. Antenna Propag.*, vol. 61, no. 2, pp. 571–577, Feb. 2013.
[47] H. Lee, J. H. Choi, C.-T. M. Wu, and T. Itoh, "A compact single radiator CRLH-inspired circularly polarized leaky-wave antenna based on substrate-integrated waveguide," *IEEE Trans. Antennas Propag.*, vol. 63, no. 10, pp. 4566–4572, Oct. 2015.
[48] C. Caloz, "Dual composite right/left-handed (D-CRLH) transmission line metamaterial," *IEEE Microw. Wireless Compon. Lett.*, vol. 16, no. 11, pp. 585–587, Nov. 2006.
[49] J. Bonache, G. Siso, M. Gil, Á. Iniesta, J. Garcia-Rincon, and F. Martin, "Application of composite right/left handed (CRLH) transmission lines based on complementary split ring resonators (CSRRs) to the design of dual-band microwave components," *IEEE Microw. Wireless Compon. Lett.*, vol. 18, no. 8, pp. 524–526, Aug. 2008.
[50] F. Bongard, J. Perruisseau-Carrier, and J. R. Mosig, "Enhanced CRLH transmission line performances using a lattice network unit cell," *IEEE Microw. Compon. Lett.*, vol. 19, no. 7, pp. 431–433, Jul. 2009.
[51] T. Jang *et al.*, "Switchable composite right/left-handed (S-CRLH) transmission line using MEMS switches," *IEEE Microw. Wireless Compon. Lett.*, vol. 19, no. 12, pp. 804–806, Dec. 2009.
[52] C. T. M. Wu, Y. Dong, J. S. Sun, and T. Itoh, "Ring-resonator-inspired power recycling scheme for gain-enhanced distributed amplifier-based CRLH-transmission line leaky wave antennas," *IEEE Trans. Microw. Theory Techn.*, vol. 60, no. 4, pp. 1027–1037, Apr. 2012.
[53] R. Keshavarz, A. Mohammadi, and A. Abdipour, "A quad-band distributed amplifier with E-CRLH transmission line," *IEEE Trans. Microw. Theory Techn.*, vol. 61, no. 12, pp. 4188–4194, Dec. 2013.
[54] T. Yang, P.-L. Chi, R. Xu, and W. Lin, "Folded substrate integrated waveguide based composite right/left-handed transmission line and its application to partial H-Plane Filters," *IEEE Trans. Microw. Theory Techn.*, vol. 61, no. 2, pp. 789–799, Feb. 2013.
[55] G. Perez-Palomino *et al.*, "Accurate and efficient modeling to calculate the voltage dependence of liquid crystal-based reflectarray cells," *IEEE Trans. Antennas Propag.*, vol. 62, no. 5, pp. 2659–2668, May 2014.
[56] A. P. Duffy, A. J. M. Martin, A. Orlandi, G. Antonini, T. M. Benson, and M. S. Woolfson, "Feature selective validation (FSV) for validation of computational electromagnetics (CEM). Part I—The FSV method," *IEEE Trans. Electromagn. Compat.*, vol. 48, no. 3, pp. 449–459, Aug. 2006.
[57] A. Orlandi, A. P. Duffy, B. Archambeault, G. Antonini, D. E. Coleby, and S. Connor, "Feature selective validation (FSV) for validation of computational electromagnetics (CEM). Part II—Assessment of FSV performance," *IEEE Trans. Electromagn. Compat.*, vol. 48, no. 3, pp. 460–467, Aug. 2006.
[58] A. Orlandi, G. Antonini, C. Ritota, and A. P. Duffy, "Enhancing feature selective validation (FSV) interpretation of EMC/SI results with grade-spread," in *Proc. IEEE Symp. Electromagn. Compat.*, Portland, OR, USA, Aug. 2006, pp. 362–367.
[59] D. E. Schaub and D. R. Oliver, "A circular patch resonator for the measurement of microwave permittivity of nematic liquid crystal," *IEEE Trans. Microw. Theory Techn.*, vol. 59, no. 7, pp. 1855–1862, Jul. 2011.

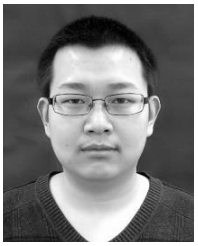

Bang-Jun Che (S'14) received the B.E. and M.E. degrees in microwave engineering from the Harbin Institute of Technology (HIT), Harbin, China, in 2012 and 2014, respectively, where he is currently pursuing the Ph.D. degree with the Department of Microwave Engineering.

His current research interests include wireless power transfer and tunable microwave device and antenna.

Mr. Che received the Student Paper Contest Award (second prize) from the 3rd IEEE Asia-Pacific Conference on Antennas and Propagation, Harbin, in 2014.

Tao Jin was born in Heilongjiang, China, in 1980. He received the B.S., M.S., and Ph.D. degrees in information and communication engineering from the Harbin Institute of Technology, Harbin, China, in 2002, 2005, and 2010, respectively.

In 2010, he joined the Faculty of Electromagnetic Field and Radio Technology, Harbin Institute of Technology, Weihai, China, as a Lecturer. His current research interests include polarimetric radar signal and data processing, high-speed digital system, and radar electronic countermeasure.

Daniel Erni (S'88–M'93) received the Diploma degree in electrical engineering from the University of Applied Sciences Rapperswil, Rapperswil, Switzerland, in 1986, and the Diploma degree in electrical engineering and the Ph.D. degree from ETH Zürich, Zürich, Switzerland, in 1990 and 1996, respectively.

He was the Founder and the Head of the Communication Photonics Group, ETH Zürich, from 1995 to 2006, where he has been with the Laboratory for Electromagnetic Fields and Microwave Electronics since 1990. Since 2006, he has been a Full Professor of General and Theoretical Electrical Engineering with the University of Duisburg–Essen, Duisburg, Germany. His current research interests include advanced data transmission schemes (i.e., O-MIMO) in board-level optical interconnects, optical on-chip interconnects, ultradense integrated optics, nanophotonics, plasmonics, quantum optics, optical and electromagnetic metamaterials, with distinct emphasis on biomedical engineering, namely for advanced RF excitation schemes in magnetic resonance imaging, numerical structural optimization into dense integrated optics device design, and science and technology studies as well as the history and philosophy of science with a distinct focus on the epistemology in engineering sciences.

Dr. Erni is a member of the Editorial Board of the *Journal of Computational and Theoretical Nanoscience,* the Center for Nanointegration Duisburg–Essen, the Applied Computational Electromagnetics Society, the Swiss Physical Society, the German Physical Society, and the Optical Society of America. He is an Associated Member of the Swiss Electromagnetics Research Centre. He is a Fellow of the Electromagnetics Academy.

Fan-Yi Meng (S'07–M'09–SM'15) received the B.S., M.S., and Ph.D. degrees in electromagnetics from the Harbin Institute of Technology, Harbin, China, in 2002, 2004, and 2007, respectively.

Since 2007, he has been with the Department of Microwave Engineering, Harbin Institute of Technology, where he is currently a Professor. He has coauthored four books, 60 international refereed journal papers, over 20 regional refereed journal papers, and 40 international conference papers. His current research interests include antennas, electromagnetic and optical metamaterials, plasmonics, and electromagnetic compatibility.

Dr. Meng was a recipient of several awards including the 2013 Top Young Innovative Talents of Harbin Institute of Technology, the 2013 CST University Publication Award, the 2010 Award of Science and Technology from the Heilongjiang Province Government of China, the 2010 "Microsoft Cup" IEEE China Student Paper Contest Award, two Best Paper Awards from the National Conference on Microwave and Millimeter Wave in China in 2009 and 2007, respectively, the 2008 University Excellent Teacher Award of the National University of Singapore, the 2007 Excellent Graduate Award of Heilongjiang Province of China, and the Outstanding Doctor Degree Dissertation Award of the Harbin Institute of Technology.

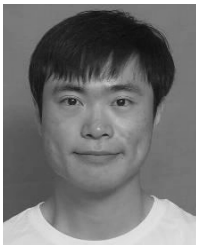

Yue-Long Lyu (S'14) received the B.E. and M.E. degrees in microwave engineering from the Harbin Institute of Technology, Harbin, China, in 2012 and 2014, respectively, where he is currently pursuing the Ph.D. degree with the Department of Microwave Engineering.

His current research interests include beam-steering antenna, tunable microwave device, and wireless power transfer.

Mr. Lyu received the Student Travel Award from the IEEE International Conference on Microwave Magnetics, Sendai, Japan, in 2014, and the Student Paper Contest Award (honorable prize) from the 3rd IEEE Asia-Pacific Conference on Antennas and Propagation, Harbin, in 2014. He was a recipient of the Outstanding Graduate of HIT in 2012 and 2014, respectively.

Qun Wu (M'93–SM'05) received the B.Sc. degree in radio engineering, the M.Eng. degree in electromagnetic fields and microwaves, and the Ph.D. degree in communication and information systems from the Harbin Institute of Technology (HIT), Harbin, China, in 1977, 1988, and 1999, respectively.

He was a Visiting Professor with Seoul National University, Seoul, South Korea, from 1998 to 1999, the Pohang University of Science and Technology, Pohang, South Korea, from 1999 to 2000, and the National University of Singapore, Singapore, from 2003 to 2010. Since 1990, he has been with the School of Electronics and Information Engineering, HIT, where he is currently a Professor and the Head with the Department of Microwave Engineering. He is also the Director of the Center for Microwaves and EMC at HIT. He has authored several books and over 100 international and regional refereed journal papers. His current research interests include electromagnetic compatibility, metamaterials, and antennas.

Prof. Wu received the Science and Technology Award from Heilongjiang Provincial Government in 2010. He was the Chair or a member in the TPC of international conferences for many times. He is a member of the Microwave Society, Chinese Institute of Electronics. He is a Technical Reviewer for several international journals. He is also the Vice Chair of the IEEE Harbin Section, and the Chair of the IEEE Harbin EMC/AP/MTT Joint Society Chapter. He has also been invited to give a keynote report or invited papers in some international conferences many times.